Schweizerischer Erdbebendienst
Service Sismologique Suisse
Servizio Sismico Svizzero
Swiss Seismological Service

ETH zürich

SITE CHARACTERIZATION REPORT

SGAK: Gampel (VS) - Kirche

Manuel Hobiger, Paolo Bergamo, Clotaire Michel, Donat Fäh

Last Modification: 19th December, 2017

Schweizerischer Erdbebendienst (SED)
Service Sismologique Suisse
Servizio Sismico Svizzero
Servizi da Terratrembels Svizzer

ETH Zürich
Sonneggstrasse 5
8092 Zürich
Schweiz
manuel.hobiger@sed.ethz.ch

Contents

1 Summary

The free-field strong-motion station SGAK was built next to the church in Gampel (VS). We performed a passive array measurement with one array configuration and additional active seismic measurements to characterize the soil underneath station SGAK in Gampel (VS), located on creek deposits at the edge of the Rhône valley.
The measurements show that the fundamental frequency of the structure beneath the station is about 2 Hz. The array measurements were analyzed with three different techniques, namely 3-component HRFK, WaveDec and SPAC. All techniques gave similar dispersion curves. The dispersion curves for the fundamental modes of both Love and Rayleigh waves could be retrieved, from around 2 to 15 Hz for the Love waves and from about 3 to 20 Hz for the Rayleigh waves. The active measurements allowed us to measure the Rayleigh wave dispersion curves up to 83 Hz for three different modes and to better constrain the very shallow subsurface through the interpretation of P-wave arrival times. Joint inversions of dispersion and ellipticity curves yielded a superficial layer of around 3 m thickness with a shear-wave velocity of about 175 m/s, followed by a second layer of around 430 m/s down to about 37 m and another layer of around 785 m/s down to 120 m, where the seismic bedrock is found. The V_{S30} value is around 377 m/s (ground type B in EC8 and C in SIA261).

2 Introduction

In the framework of the second phase of the Swiss Strong Motion Network (SSMNet) renewal project, a new station was planned in Gampel (VS). The site selection resulted in the church as the best site from risk and noise aspects. The new station, called SGAK, was constructed on the area of the church, close to the cemetary and went operational on 30 May 2016. The location of the station is shown in Fig. 1.

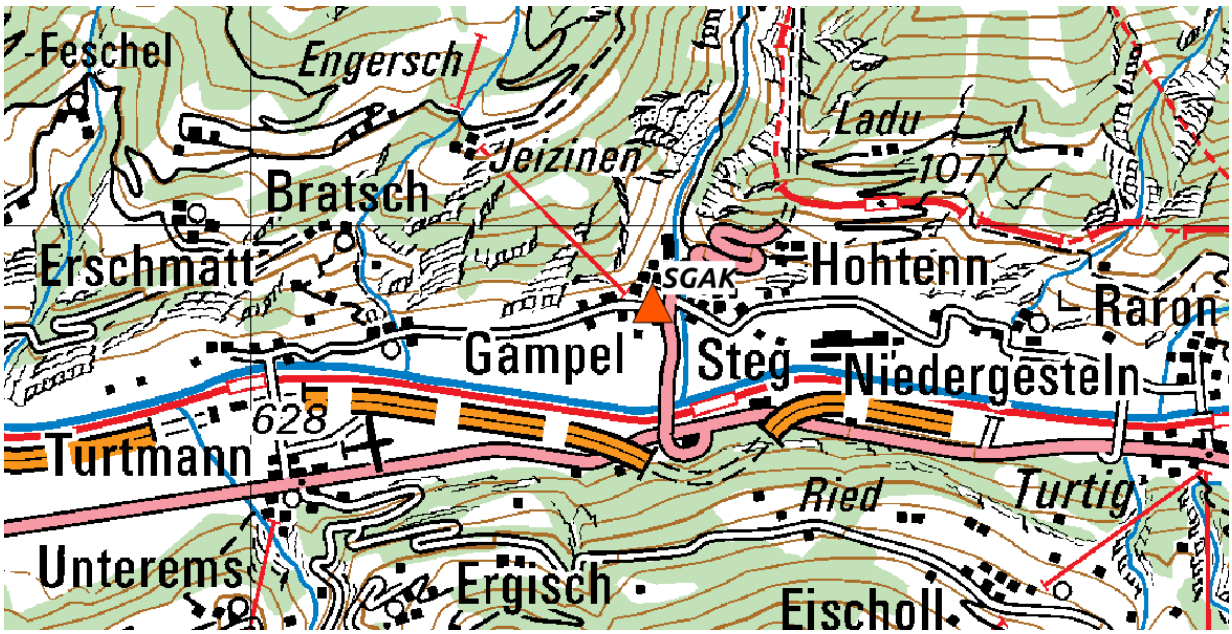

Figure 1: Map showing the location of station SGAK in Gampel.

3 Geological setting

A geological map of the surroundings of station SGAK is shown in Fig. 2. The station is located on creek deposits close to the edge of the Rhône river basin.

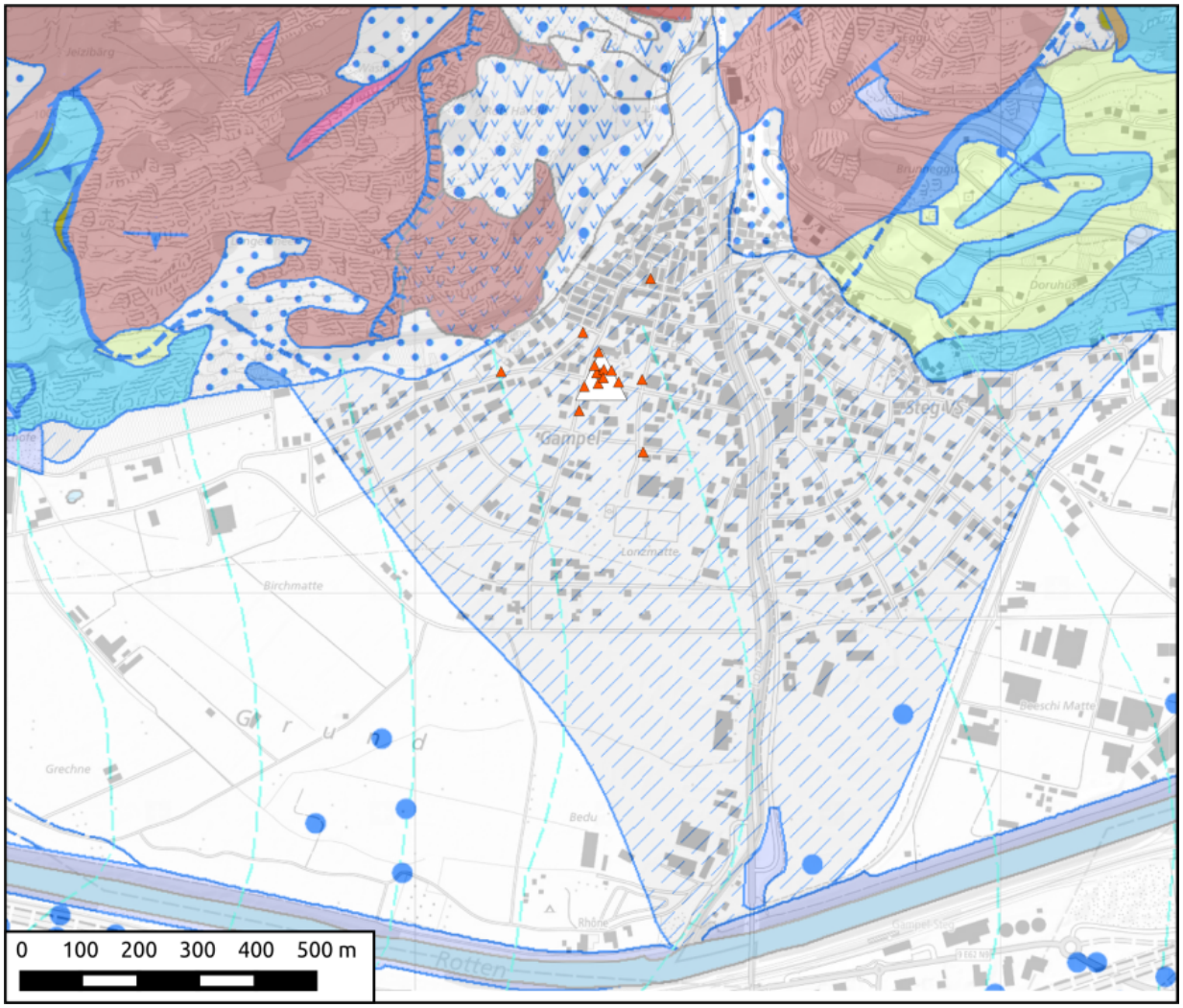

Figure 2: Geological map of the area around station SGAK. According to the geological atlas, station SGAK and all stations of the passive array measurement lie on creek deposits (grey area with blue dashes). The white area corresponds to alluvial deposits of the Rhône river, the red color corresponds to granite and granodiorite formations. Green corresponds to moraine, light blue to limestone and dark blue to dogger.

4 Site characterization

4.1 Measurements and data set

In order to characterize the local underground structure around station STHK, passive and active seismic array measurements were carried out on 8 November 2016. The layout of the seismic measurements is shown in Fig. 3.
For the passive seismic measurements, a single large array of stations was installed. It was planned to consist of a central station and five rings with radii of 8, 18, 36, 78 and 170 m, respectively, with three stations per ring and a rotation between the different rings. The station names of this array are composed of "SGAK" followed by a two-digit number between 42 and 49, 52 and 55, 63 to 65 and 68 (corresponding to the Centaur digitizer serial number for sensors connected to channel A and serial number plus 20 for sensors connected to channel B). The minimum interstation distance in the array was 6.7 m, the maximum distance 300.4 m. The array recording time was 185 minutes (or 11100 s).
The station locations have been measured by a differential GPS system (Leica Viva GS10) which was set up to measure with a precision better than 5 cm. For all station locations except one this precision was achieved. Station SGAK54 on the outermost ring was set up in the town center surrounded by buildings. For this station, the measurement precision was only 1.0 m. For the active seismic measurment, a straight line of 16 three-component geophones (corner frequency 4.5 Hz) was deployed in close proximity to station SGAK (green line in Fig. 3). The regular spacing between the geophones was set to 1.6 m, for a total length of the linear spread of 24 m. As seismic source, we used a 5-kg sledgehammer hitting a flat metal plate. The source was positioned at five different locations; at 5.5 and 4.7 m offset south of the spread, at the center and at the two extremities of the geophone array. At each shooting postion, 10 hammer blows were repeated.

Table 1: List of the passive seismic array measurements in Gampel.

Array name	Number of sensors	Minimum interstation distance [m]	Maximum interstation distance [m]	Recording time [s]
1	16	6.7	300.4	11100

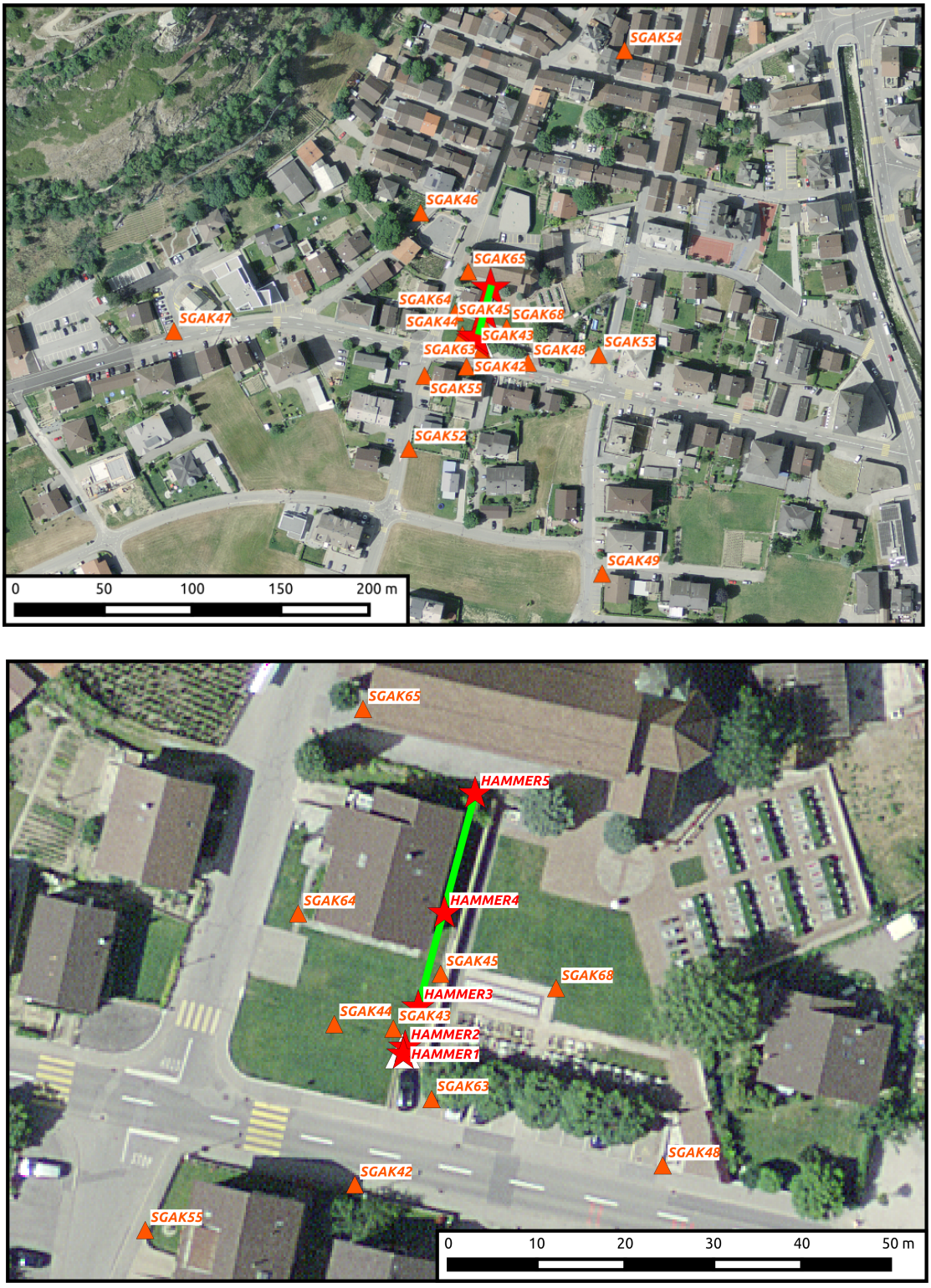

Figure 3: Layout of the array measurements around station SGAK. The location of SGAK is indicated by the white triangle, the locations of the stations for the passive seismic measurement by the orange triangles. The shot points of the active measurement are indicated by red stars and the geophone line by the green line. ©2017 swisstopo (JD100042)

4.2 Measurement results

4.2.1 H/V curves

Figure 4 shows the H/V curves determined with the time-frequency analysis method (Fäh et al., 2009) for all stations of the passive array and a map of the fundamental frequencies. All curves show a clear peak around 2 Hz. Stations close to the northwestern edge of the array show higher fundamental frequencies, corresponding to a shallower sedimentary cover. Stations to the southeast, where the sedimentary cover is thickening, show lower fundamental frequencies. In the array center, values between 1.9 and 2.0 Hz are observed.

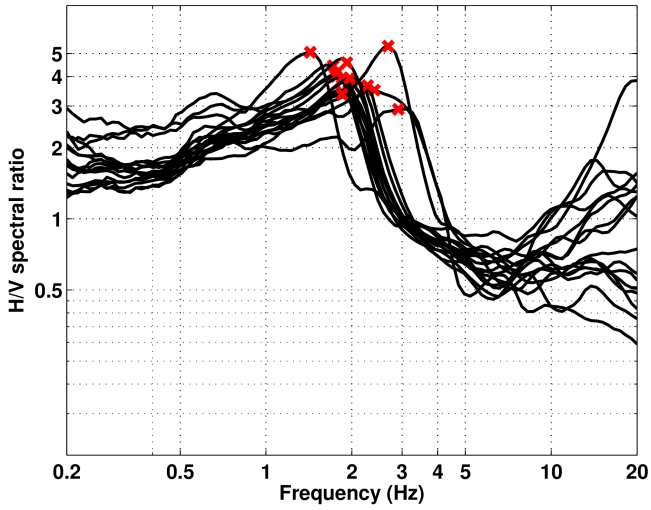

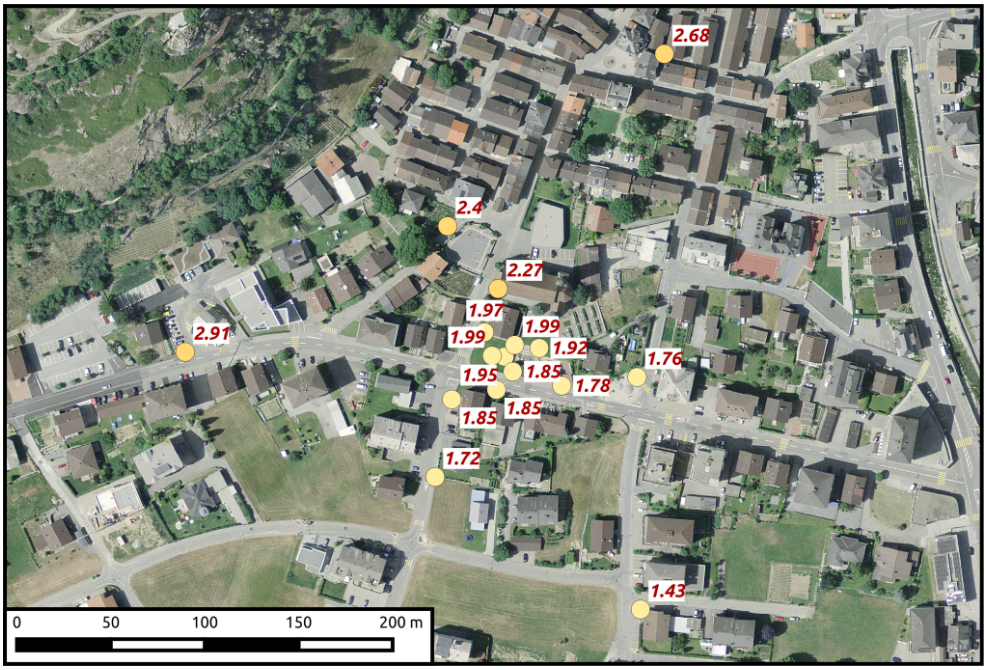

Figure 4: Overview of the H/V measurements for the different stations of the array measurement in Gampel (top) and map with the fundamental frequencies (bottom).

4.2.2 RayDec ellipticity curves

The RayDec technique (Hobiger et al., 2009) is meant to eliminate the contributions of other wave types than Rayleigh waves and give a better estimate of the ellipticity than the classical H/V technique. The RayDec ellipticity curves for all stations of the array measurements are shown in Fig. 5.
The RayDec curves are similar to the H/V curves and also show the same variability of the fundamental frequency, with stations in the northwest having larger fundamental frequencies. The RayDec curve of station SGAK43, the station in the array center and closest to SGAK, will be used as ellipticity target for the inversion.

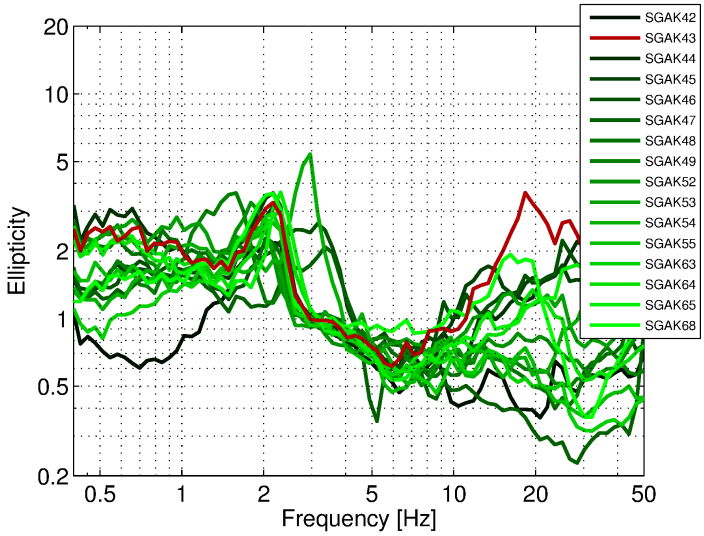

Figure 5: RayDec ellipticities for all measurement stations.

4.2.3 Polarization measurements

The polarization analysis was performed according to Burjánek et al. (2010) and Burjánek et al. (2012). The results for all stations of the array are similar. Only the results for SGAK43, the station in the array center and closest to SGAK, are shown here.
There is no preferential linear particle polarization visible, but there is a preferential strike direction perpendicular to the valley axis below 1 Hz. This might be due to the 2-dimensional polarization of the Rhône valley, but the effect does not seem to be very pronounced, as it is not visible in the H/V measurements.

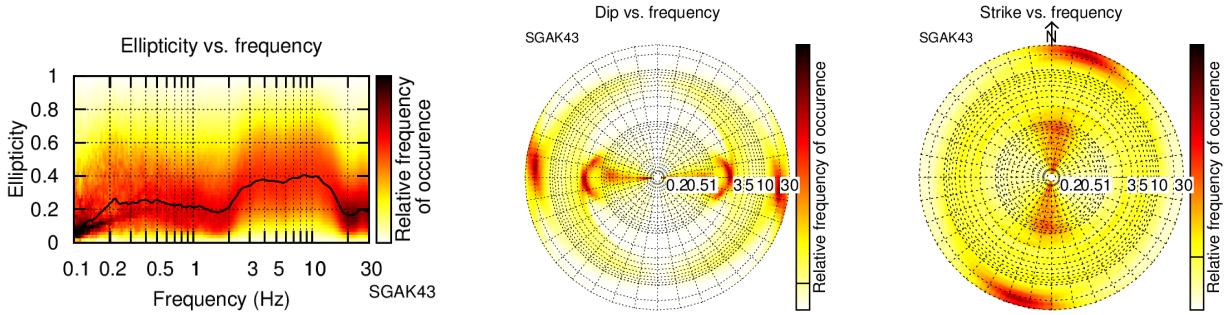

Figure 6: Polarization analysis of station SGAK43.

4.2.4 3-component high-resolution FK

The results of the 3-component high-resolution FK analysis (Poggi and Fäh, 2010) are shown in Fig. 7. On the transverse component, a Love wave dispersion curve is clearly visible between 2.2 and 21.4 Hz. Higher modes are hardly visible and were not picked. On the vertical component, a dispersion curve can be clearly identified within the array resolution limits between 2.7 and 23.6 Hz. On the radial component, the same dispersion curve can be retrieved, but only above 5 Hz. Some parts of higher modes might be visible at higher velocities, but they remain more unclear.
The corresponding ellipticity curves of the fundamental modes on the vertical and radial components can be clearly identified.

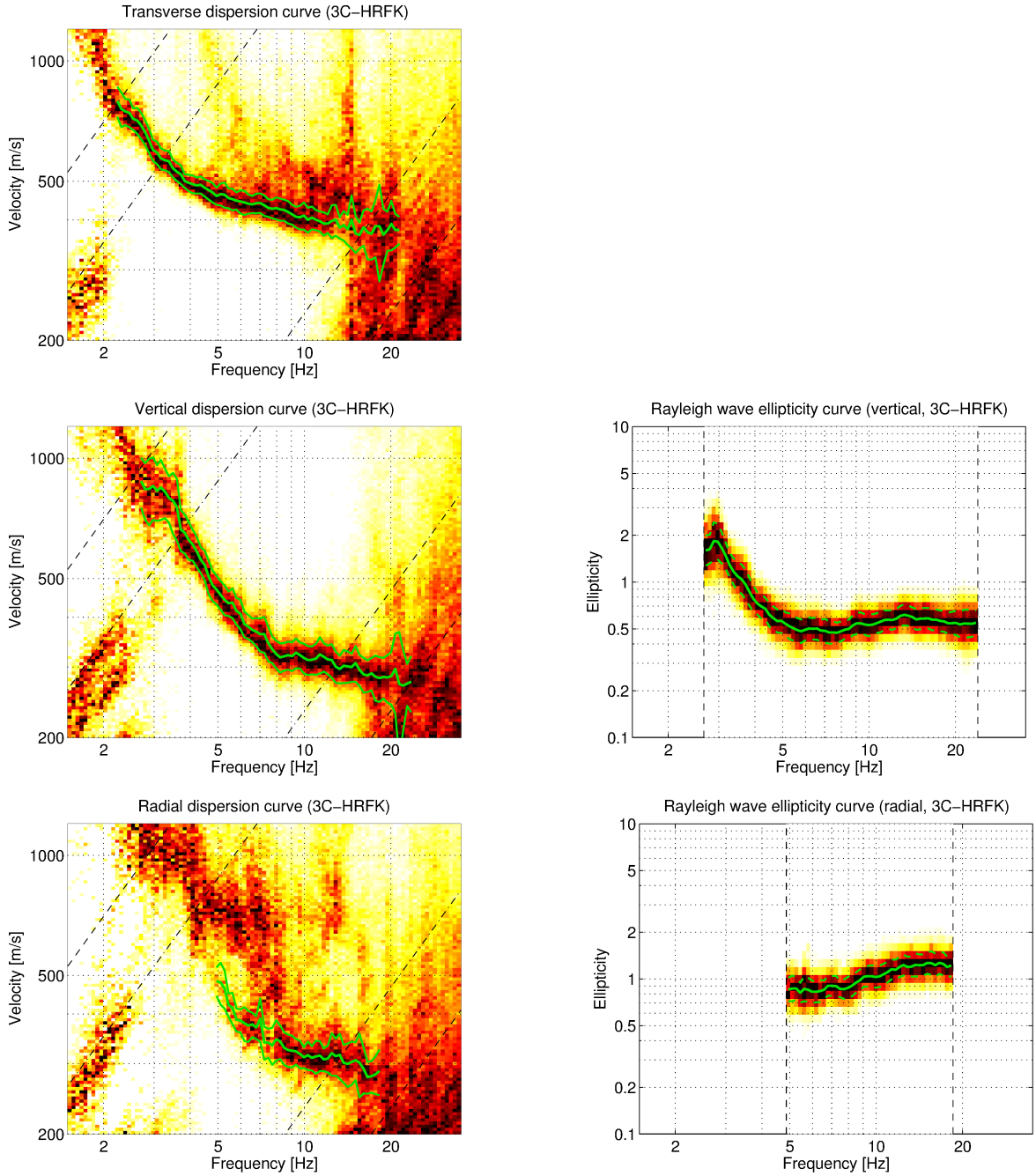

Figure 7: Dispersion and ellipticity curves obtained with the 3-component HRFK algorithm (Poggi and Fäh, 2010). In the left column, the dispersion curves for the transverse, vertical and radial components are shown. On the right side, the corresponding ellipticity curves for the vertical and radial components are displayed. The dashed and dotted black lines are the array resolution limits. The solid green lines are picked from the data, where the central line indicates the best values and the two outer lines the standard deviation.

4.2.5 WaveDec

The results of the WaveDec (Maranò et al., 2012) processing are shown in Fig. 8. This technique estimates the properties of single or multiple waves simultaneously with a maximum likelihood approach. In order to get good results, the parameter γ, which modifies the sharpness of the wave property estimation, has been tuned. Here, a value of $\gamma = 0.2$ was used.
The Love wave dispersion curve is clearly retrieved between 2.2 and 10.0 Hz. The Rayleigh wave disersion curve is picked between 3.3 and 14.7 Hz. The ellipticity angle for the picked Rayleigh wave dispersion curve is always negative, indicating retrograde particle motion. At low frequencies, the ellipticity values are increasing, but the peak frequency is outside of the array resolution limits. Anyhow, retrograde particle motion at the right flank of the peak would indicate that there is no singularity in the ellipticity curve and thus no large impedance contrast.

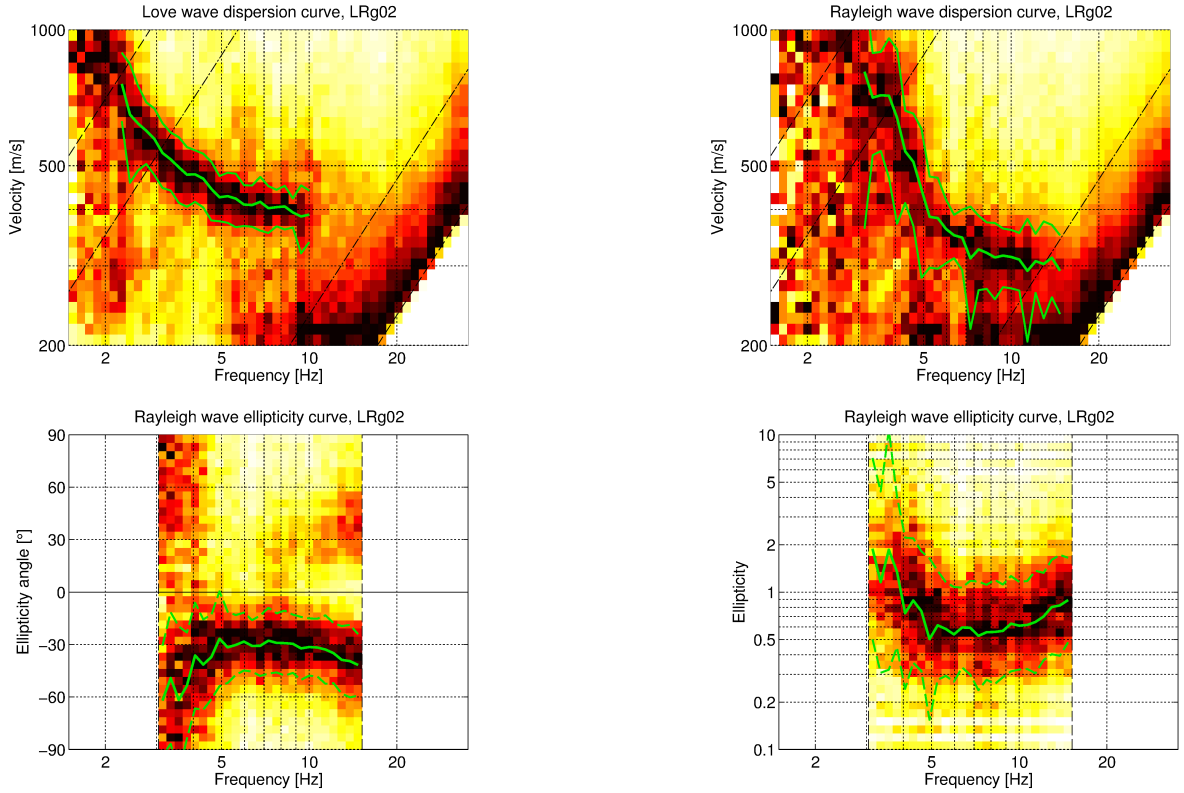

Figure 8: Love and Rayleigh wave dispersion and ellipticity curves obtained with the WaveDec technique (Maranò et al., 2012). The dashed lines indicate the theoretical array resolution limits. Top line: Love wave (left) and Rayleigh wave (right) dispersion curves. Bottom line: Rayleigh wave ellipticity curve represented as ellipticity angle (left), Rayleigh wave ellipticity (right), i.e. the absolute value of the tangent of the ellipticity angle.

4.2.6 SPAC

The SPAC (Aki, 1957) curves of the vertical components have been calculated using the M-SPAC (Bettig et al., 2001) technique implemented in geopsy. Rings with different radius ranges had been defined previously and for all station pairs with distance inside this radius range, the cross-correlation was calculated in different frequency ranges. These cross-correlation curves are averaged for all station pairs of the respective ring and give the SPAC curve. The rings are defined in such a way that at least three station pairs contribute and that their connecting vectors have a good directional coverage.
The SPAC curves for all defined rings are shown in Fig. 9. The black points indicate the data values which contributed to the final dispersion curve estimation, which was made with the function `spac2disp` of the geopsy package. These resulting dispersion curves are also shown in Fig. 9.
Using SPAC, we can pick a Rayleigh wave dispersion curve between 1.5 and 14.1 Hz.

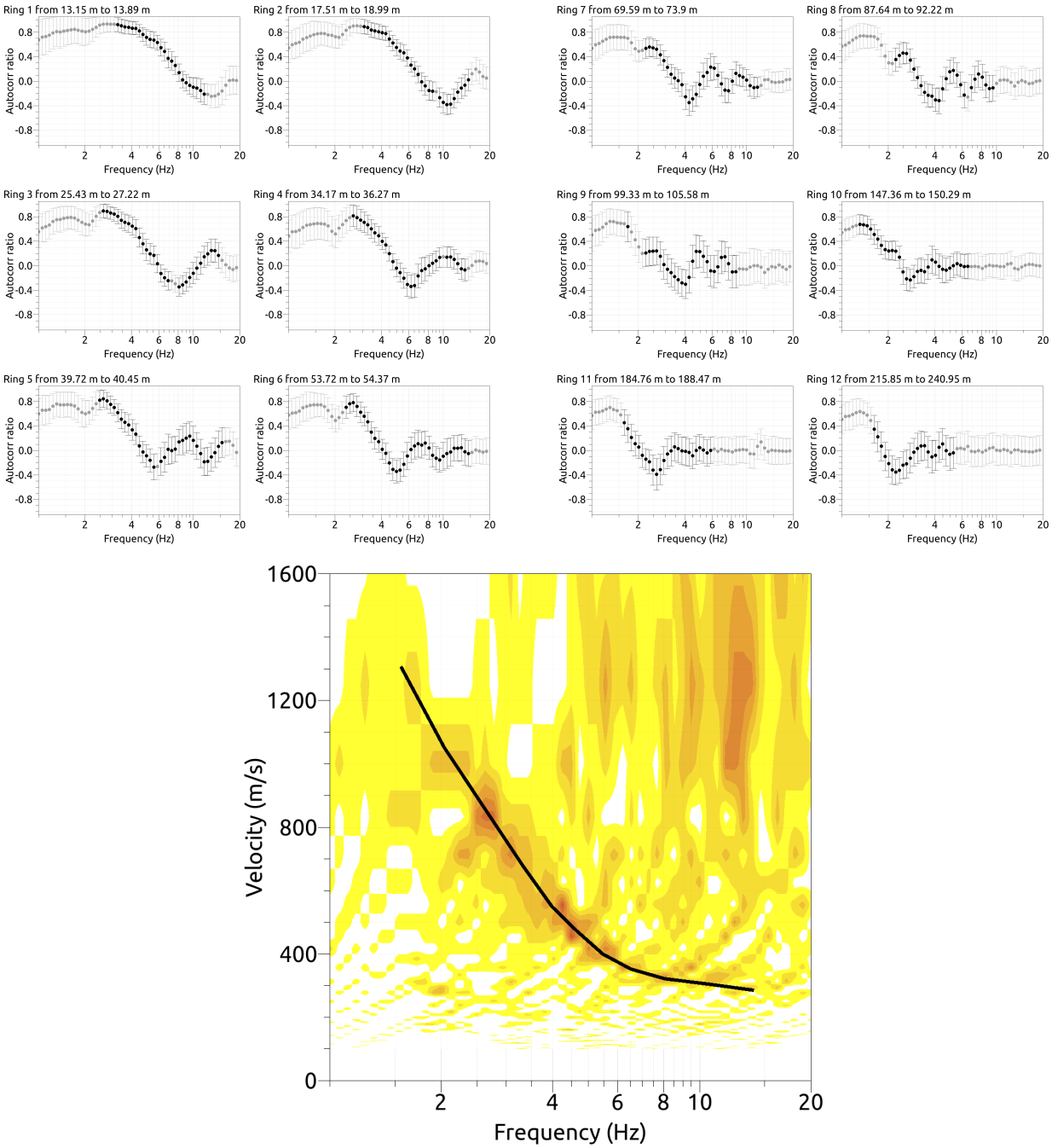

Figure 9: Top: SPAC curves, the black data points contributed to the dispersion curve estimation. Bottom: Resulting Rayleigh wave velocities. The black line corresponds to the picked dispersion curve.

4.3 Active measurement results

4.3.1 Seismic refraction

The sesmic sections acquired with the geophone array were first processed using the seismic refraction analysis (Redpath, 1973). The vertical component seismograms referring to the same shooting position were stacked and P-wave first-break arrival times were manually picked. The obtained five hodocrones (one from each shooting point) do not show significant lateral variations and were hence collapsed in a single travel-time curve as a function of the offset (Fig. 10). This curve was interpreted with the intercept-time method; direct and refracted arrivals at the different geophone locations are well explained by a three-layer model at the shallow surface (see Fig. 10), with P-wave velocities of 339 m/s, 651 m/s and 811 m/s, respectively, and layer interfaces at 2.4 m and 5.5 m depth, respectively. The values for the thickness and the P-wave velocities determined by refraction will be used to fix the superficial structure in the inversions.

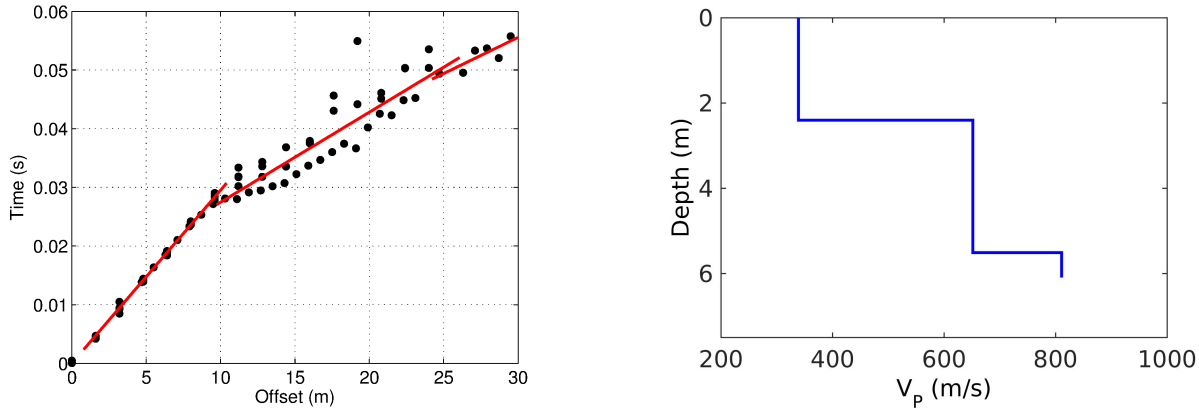

Figure 10: Left: Results of the seismic refraction analysis using the shotpoints HAMMER1, HAMMER2, HAMMER3, HAMMER4 and HAMMER5. The P-wave first-break arrival times at the different geophones can be explained by three layers at the shallow surface. Right: Corresponding P-wave velocity profile.

4.3.2 MASW

Vertical and longitudinal component seismic traces, acquired with shooting positions at HAMMER1 and HAMMER2, were processed with the MASW technique (Park et al., 1999). The acquired seismograms were first translated to the frequency-wavenumber domain applying a 2D f-k transform Socco and Strobbia (2004); f-k images belonging to the same hammering location and same component were then summed, and energy maxima were manually selected on these stacked panels. As a result, we obtain four Rayleigh wave dispersion curves (from vertical or longitudinal component, and from shooting position HAMMER1 or HAMMER2), which are shown in Fig. 11. These curves show good reciprocal consistency, and include three different modes identified as the fundamental, first and second higher modes.

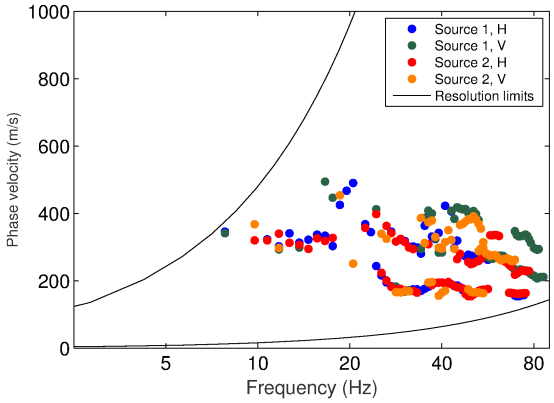

Figure 11: Results of the MASW analysis. The Rayleigh wave dispersion curves were obtained from the processing of the vertical (V) and longitudinal (H) components of the seismic sections relevant to shooting positions HAMMER1, HAMMER2.

4.4 Summary

Fig. 12 gives an overview of the dispersion and ellipticity curves determined by the different methods.
For Love waves, the HRFK and WaveDec results for the respective arrays are in good agreement, with slightly lower velocities determined by WaveDec.
For the Rayleigh waves, there is a very good agreement between the different methods. The dispersion curve measured with SPAC exceeds the lower frequency limit of the array. For the fundamental Rayleigh wave mode, all curves measured using different methods give similar results and we can determine the dispersion curve over the complete accessible frequency range between the array resolution limits. The measurement with the active seismic source extends the range of the dispersion curve to higher frequencies, up to about 75 Hz. Two additional modes are also measured with the active experiment, which we interpret as the first and second harmonic modes, respectively. They reach 86 and 83 Hz, respectively.
The ellipticity curves retrieved using the array methods (WaveDec and vertical component of HRFK) are in good agreement, the HRFK of the radial component differs from it. As stated earlier, the WaveDec curve is retrograde over the whole accessible frequency range, indicating that there is no singularity at the fundamental frequency. The RayDec ellipticity curve from station SGAK43 in the center of the array differs from the ellipticity curves obtained with the array methods, as the curve is shifted around the peak frequency. This may be caused by the differences in the H/V and ellipticity curves of the different array stations. We assume that the RayDec curve measured at the center of the array is more representative of the true ellipticity function there than the array curves which are somehow averaged over a multitude of stations and are based on the farthest station pairs at the lowest accessible frequencies, i.e. correspond to station pairs including the stations closest to the valley edge where the fundamental frequency increases.

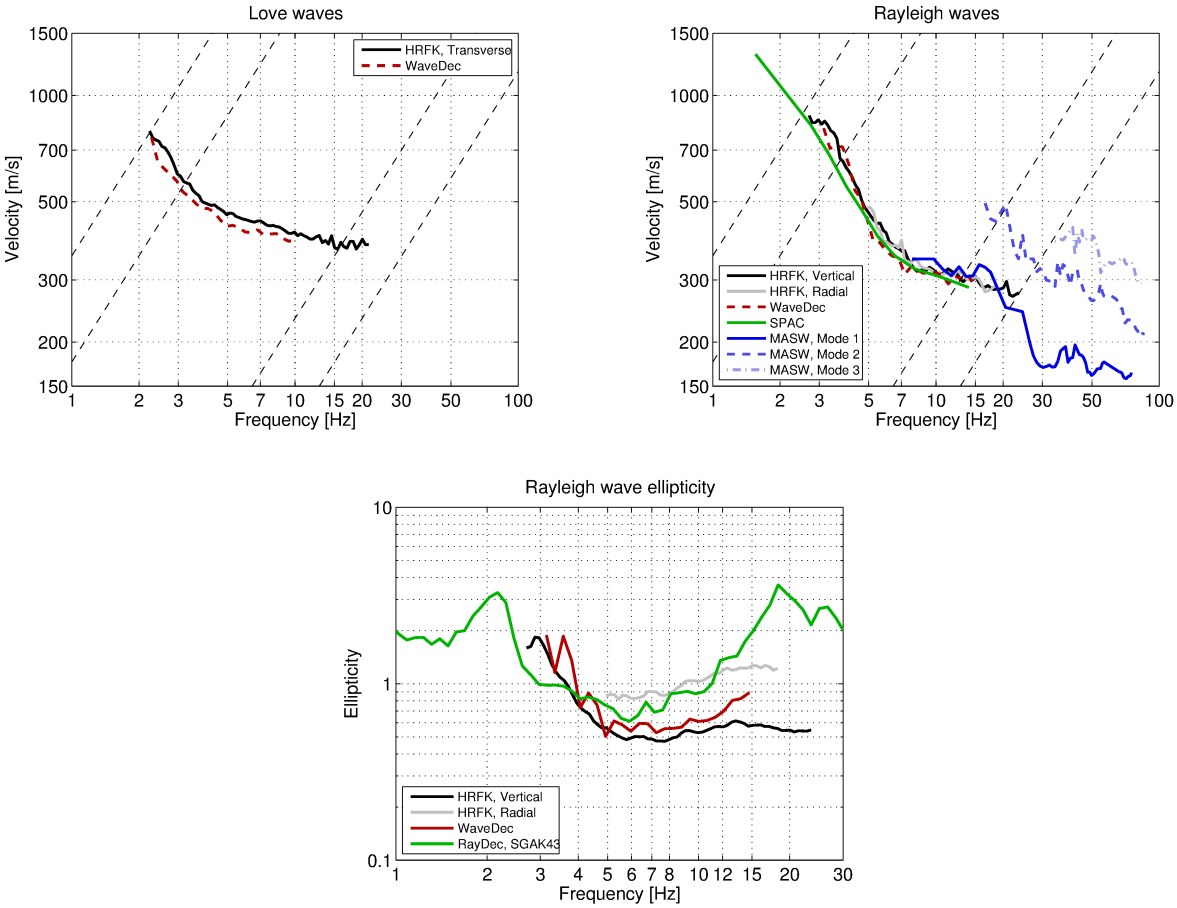

Figure 12: Overview of the Love and Rayleigh wave dispersion curves as well as the ellipticity curves for both arrays. The dashed lines indicate the theoretical resolution limits of the array. The RayDec ellipticity curve corresponds to station SGAK43.

5 Data inversion

5.1 Inversion targets

We performed inversions using as much information as possible as inversion targets. The Rayleigh and Love wave dispersion curves measured with HRFK were assumed to correspond to the respective fundamental modes. The MASW curves of the fundamental mode were taken in the higher frequency part only, i.e. above 24.4 Hz. The two other modes detected with MASW were taken as the first and second higher harmonic modes. For the ellipticity target, the whole area of the peak was used, following the recommendations of Hobiger et al. (2013) for ellipticity curves without singularities. The details of the inversion targets are indicated in Table 2 and the corresponding curves are shown in Fig. 13.

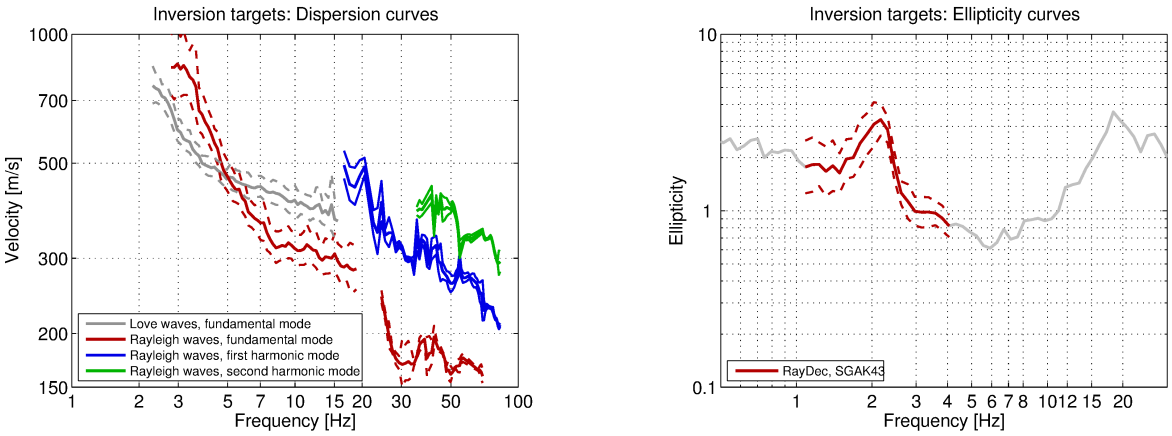

Figure 13: Overview of the dispersion (left) and ellipticity (right) curves used as targets for the different inversions.

Table 2: List of the data curves used as target in the inversion.

Method	Wave type	Mode	Curve type	Frequency range [Hz]
HRFK (T)	Love	fundamental	dispersion	2.3 - 15.2
HRFK (V)	Rayleigh	fundamental	dispersion	2.8 - 18.4
MASW	Rayleigh	fundamental	dispersion	24.4 - 68.7
MASW	Rayleigh	first higher	dispersion	16.7 - 82.9
MASW	Rayleigh	second higher	dispersion	35.5 - 82.9
RayDec (SGAK43)	Rayleigh	fundamental	ellipticity	1.09 - 4.1

5.2 Inversion parameterization

For the inversion, six different parameterizations have been used in total. The first five had free values of the depths and velocities of the different layers, ranging from four to eight layers (including half-space). The last parameterization had fixed layer depths and consisted of 20 layers in total. According to the P-wave refraction results, the first layer has a depth of 2.4 m and a P-wave velocity of 340 m/s, followed by a second layer with a thickness of 3.1 m and a V_P of 650 m/s. The V_P values of the uppermost two layers were consequently fixed to these values, the depth of the first layer was allowed to range from 2 to 3 m, the one of the second layer between 5 and 6 m. For the lower layers, P-wave velocities were allowed to vary up to 5000 m/s. The S-wave velocities were allowed to range from 50 to 3500 m/s. The deepest layers were parameterized to range to a depth of 200 m. The density was fixed to 2 300 kg/m^3 for the lowest layer and to 2 000 kg/m^3 for all other layers. For the inversion with only four layers, the depth values of the different layers were allowed to vary more freely to enable a good fitting of the data.

5.3 Inversion results

We performed a total of six inversions with different parameterizations (see Table 3). Each inversion run produced 200 000 total models in order to assure a good convergence of the solution. The results of these inversions are shown in Figs 14 - 19.
For the different inversion targets, all inversions with five to eight layers yielded very similar minimum misfit values. This indicated that they all fitted the data comparably well, but the best models may still slightly differ. The inversion using only four layers has a higher misfit, certainly because the model does not have enough complexity to explain the data. Using the fixed layer approach, the minimum misfit was also higher. This can be due to either an incomplete conversion to the final model or to the missing of appropriate interface depths in the parameterization.
With the four-layer approach, especially the fundamental Rayleigh wave dispersion curve was badly fitted. With the other parameterizations, all target curves are well fitted, with some deviations at the low and high frequency ranges of the used Love wave dispersion curve.

Table 3: List of inversions

Inversion	Number of layers	Number of models	Minimum misfit
SGAK4l	4	200 000	1.164
SGAK5l	5	200 000	0.986
SGAK6l	6	200 000	1.005
SGAK7l	7	200 000	1.038
SGAK8l	8	200 000	1.059
SGAKfix	20	200 000	1.326

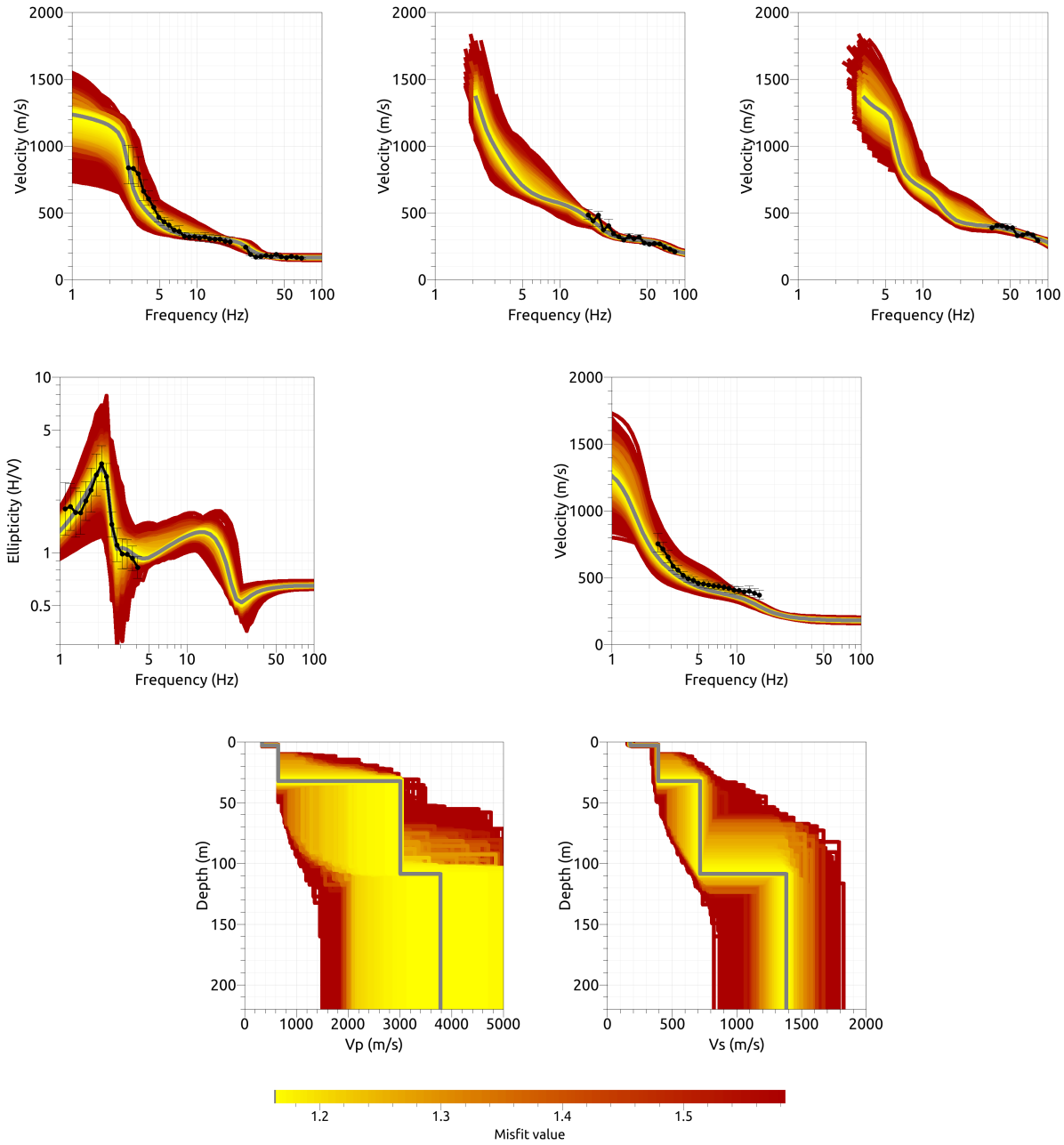

Figure 14: Inversion SGAK4l. Top line: Dispersion curves for the Rayleigh wave fundamental mode (left), first harmonic mode (center) and second harmonic mode (right). Center line: Ellipticity curve of the Rayleigh wave fundamental mode (left) and dispersion curve of the Love wave fundamental mode (right). Bottom line: P-wave velocity profiles (left) and S-wave velocity profiles (right). The black dots indicate the data points used for the inversion, the gray line indicates the best-fitting model.

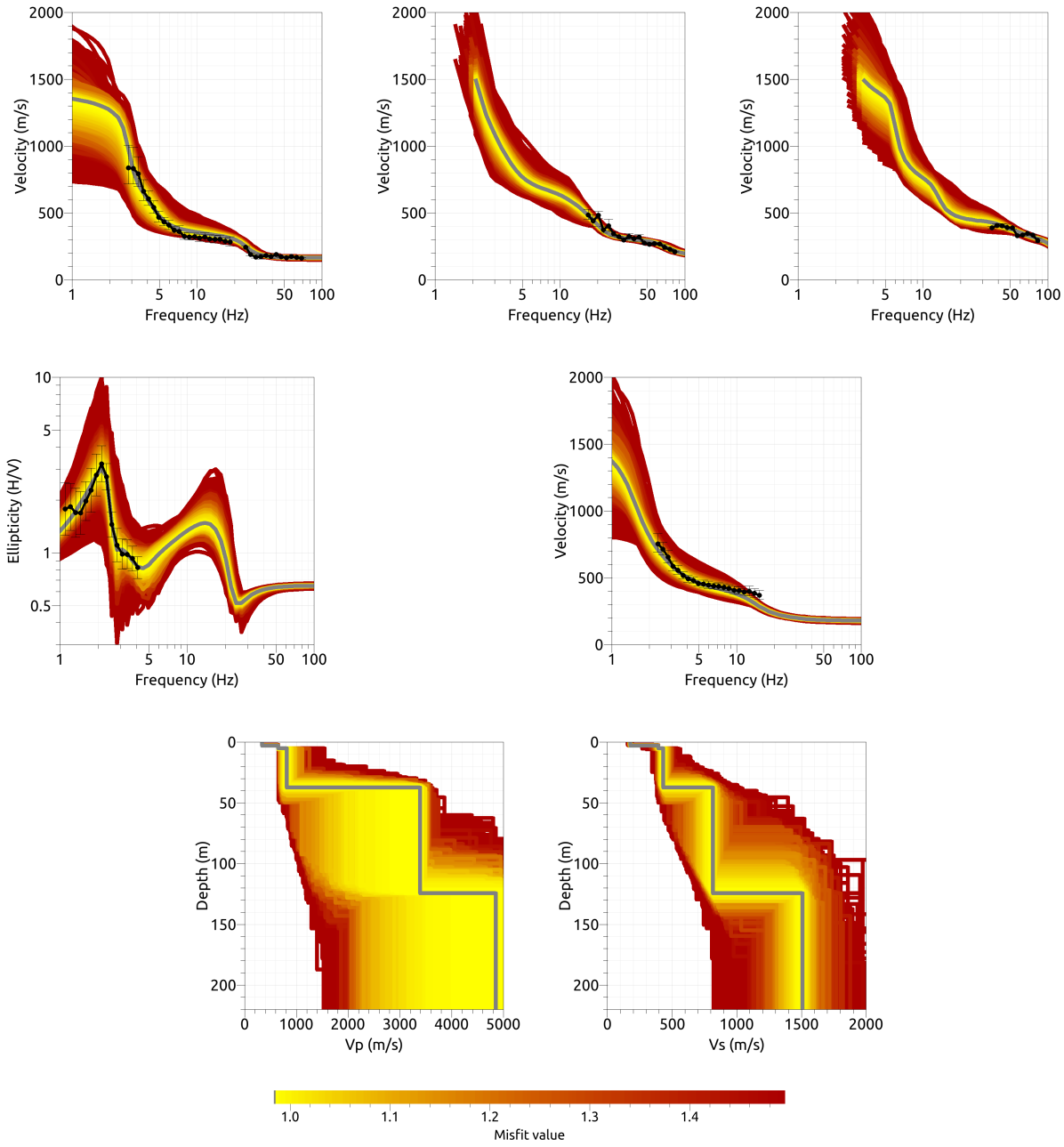

Figure 15: Inversion SGAK5l. Top line: Dispersion curves for the Rayleigh wave fundamental mode (left), first harmonic mode (center) and second harmonic mode (right). Center line: Ellipticity curve of the Rayleigh wave fundamental mode (left) and dispersion curve of the Love wave fundamental mode (right). Bottom line: P-wave velocity profiles (left) and S-wave velocity profiles (right). The black dots indicate the data points used for the inversion, the gray line indicates the best-fitting model.

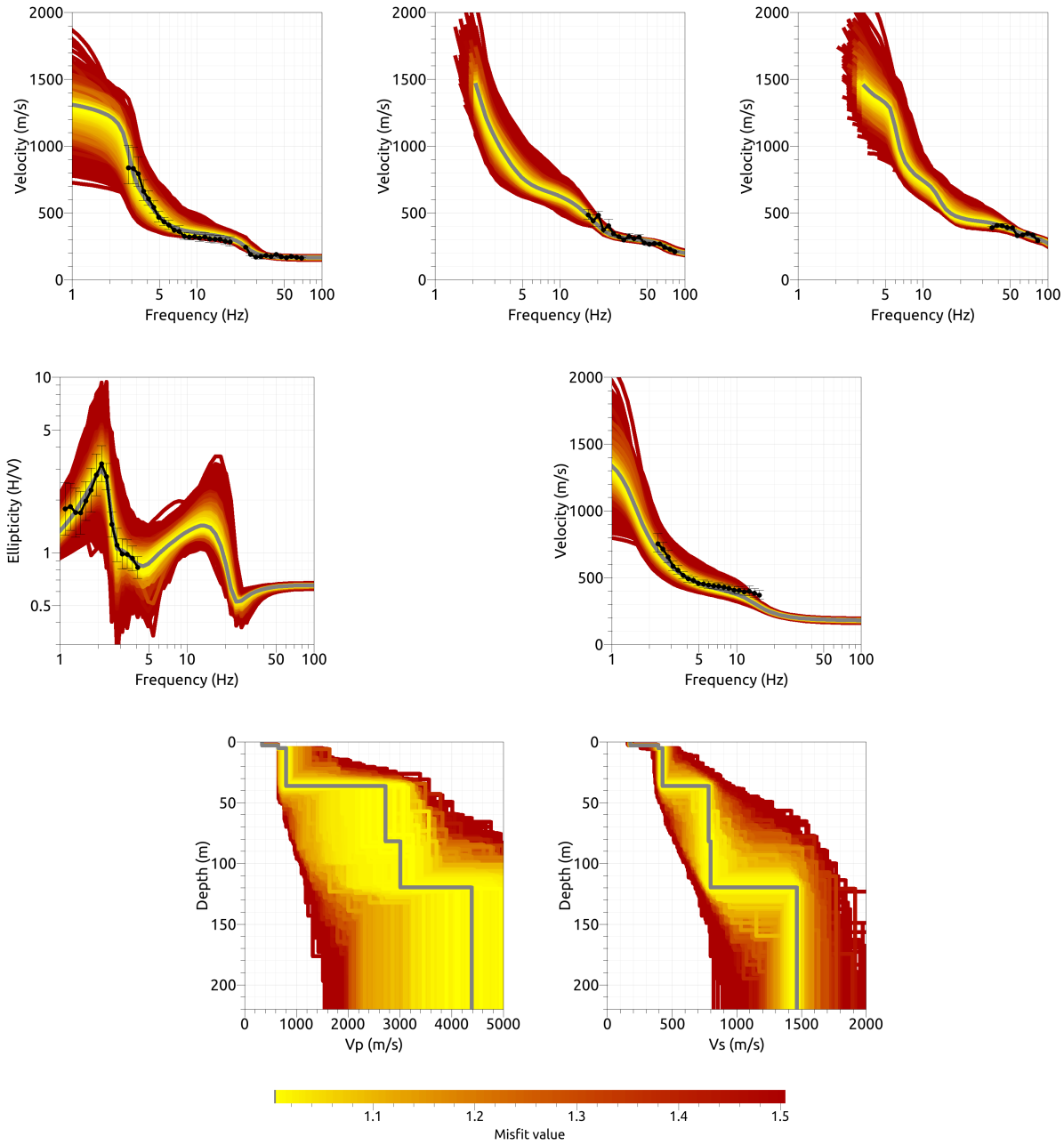

Figure 16: Inversion SGAK6l. Top line: Dispersion curves for the Rayleigh wave fundamental mode (left), first harmonic mode (center) and second harmonic mode (right). Center line: Ellipticity curve of the Rayleigh wave fundamental mode (left) and dispersion curve of the Love wave fundamental mode (right). Bottom line: P-wave velocity profiles (left) and S-wave velocity profiles (right). The black dots indicate the data points used for the inversion, the gray line indicates the best-fitting model.

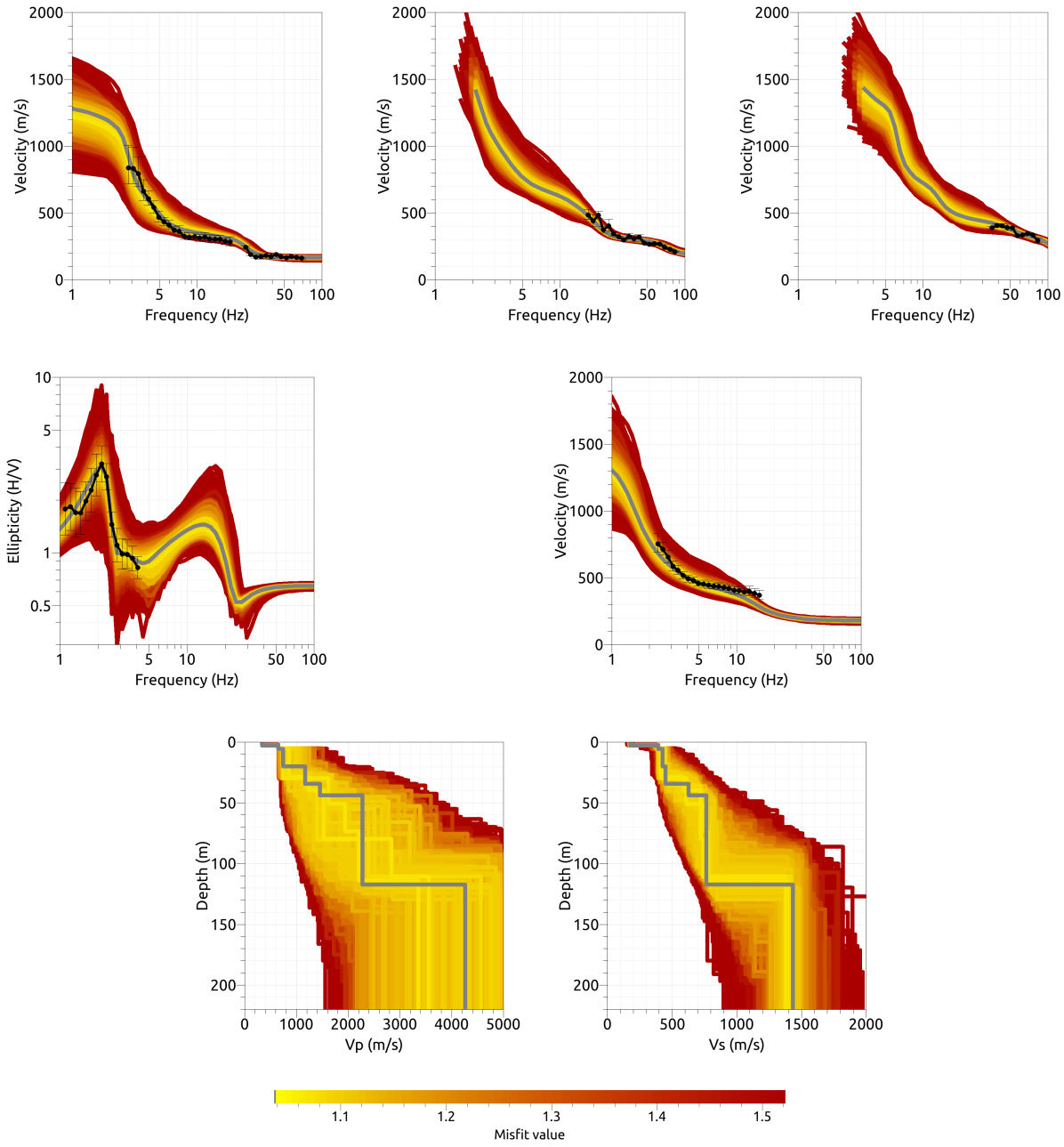

Figure 17: Inversion SGAK7l. Top line: Dispersion curves for the Rayleigh wave fundamental mode (left), first harmonic mode (center) and second harmonic mode (right). Center line: Ellipticity curve of the Rayleigh wave fundamental mode (left) and dispersion curve of the Love wave fundamental mode (right). Bottom line: P-wave velocity profiles (left) and S-wave velocity profiles (right). The black dots indicate the data points used for the inversion, the gray line indicates the best-fitting model.

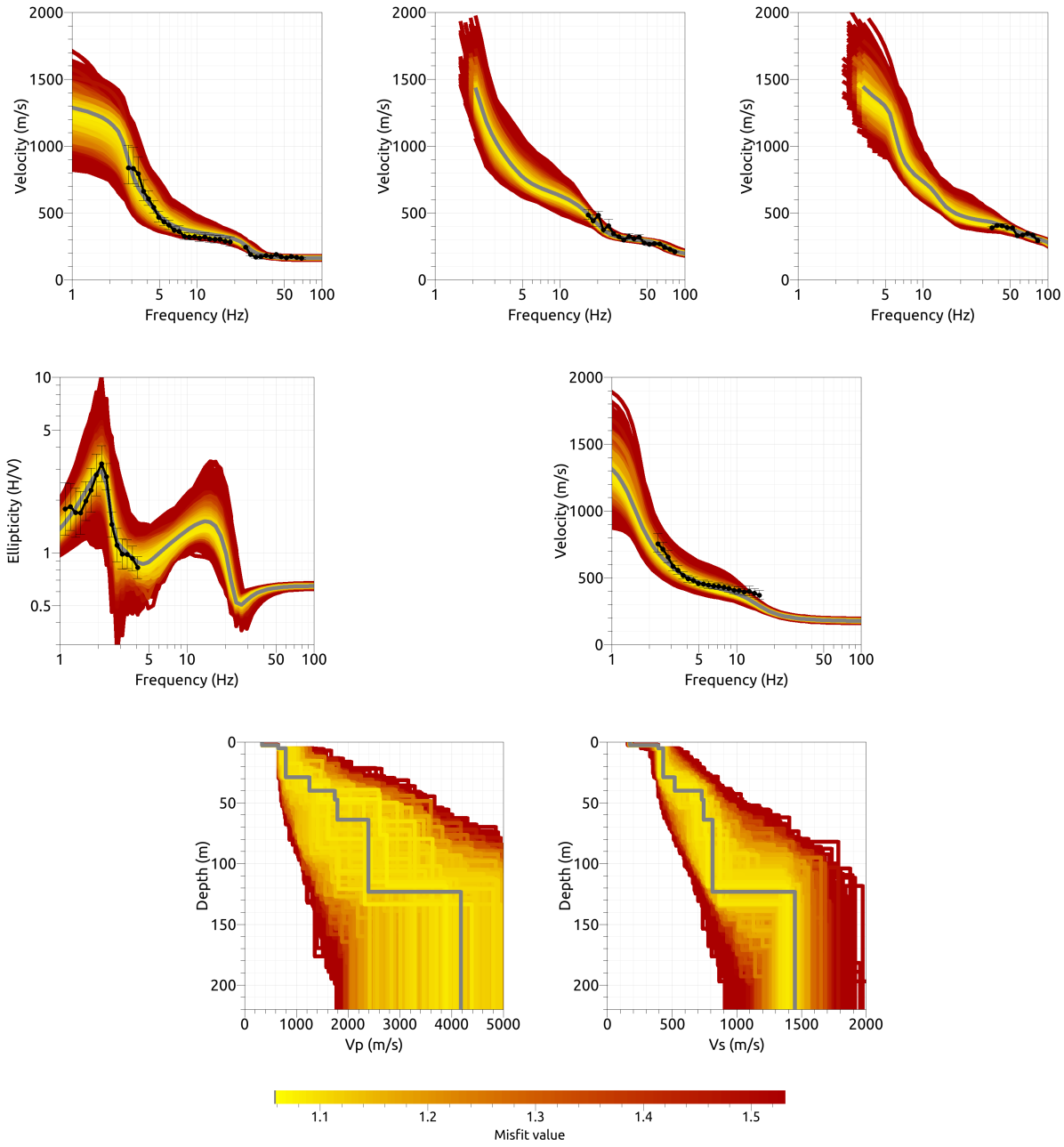

Figure 18: Inversion SGAK8l. Top line: Dispersion curves for the Rayleigh wave fundamental mode (left), first harmonic mode (center) and second harmonic mode (right). Center line: Ellipticity curve of the Rayleigh wave fundamental mode (left) and dispersion curve of the Love wave fundamental mode (right). Bottom line: P-wave velocity profiles (left) and S-wave velocity profiles (right). The black dots indicate the data points used for the inversion, the gray line indicates the best-fitting model.

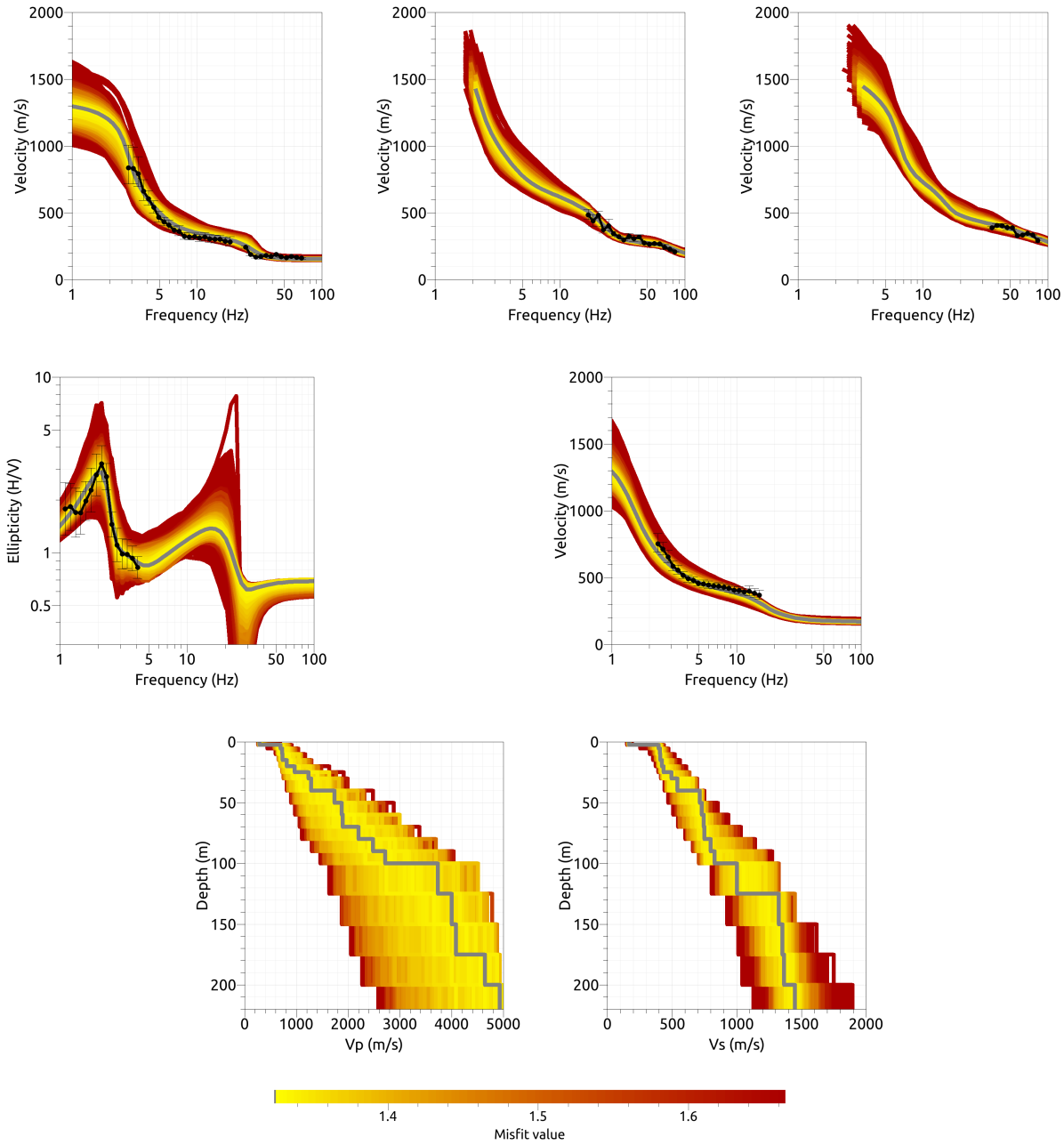

Figure 19: Inversion SGAKfix. Top line: Dispersion curves for the Rayleigh wave fundamental mode (left), first harmonic mode (center) and second harmonic mode (right). Center line: Ellipticity curve of the Rayleigh wave fundamental mode (left) and dispersion curve of the Love wave fundamental mode (right). Bottom line: P-wave velocity profiles (left) and S-wave velocity profiles (right). The black dots indicate the data points used for the inversion, the gray line indicates the best-fitting model.

5.4 Discussion of the inversion result

The best-fitting models of the inversions are shown in Fig. 20. Down to about 20 m, all models are virtually identical. They differ in the deeper parts. The models with more than four layers show a first significant interface at depths of about 37 m and a second one at around 120 m. The fixed-layer model is similar, but smoother. The model with only four layers shows these interfaces at lower depths of about 32 and 109 m, respectively. The general S-wave velocity profile can be described as follows: the S-wave velocity of the first layer with a thickness of about 3 m is approximately 175 m/s. Models with five or more layers show a second layer with a v_S of about 395 m/s down to about 5 m. The next layer is mainly characterized by a v_S of 430 m/s down to about 37 m of depth. The next layer has a v_S of around 785 m/s down to about 120 m, where the seismic bedrock with an S-wave velocity of about 1500 m/s starts.
The V_{S30} value for the inversion with four layers is 353.2 m/s, for the other inversions it ranges from 373.6 to 381.1 m/s (average value 377.6 $\pm$ 2.8 m/s). This corresponds to soil class B in EC8 and C in SIA261. We select the inversions with over four layers as representative for the structure.

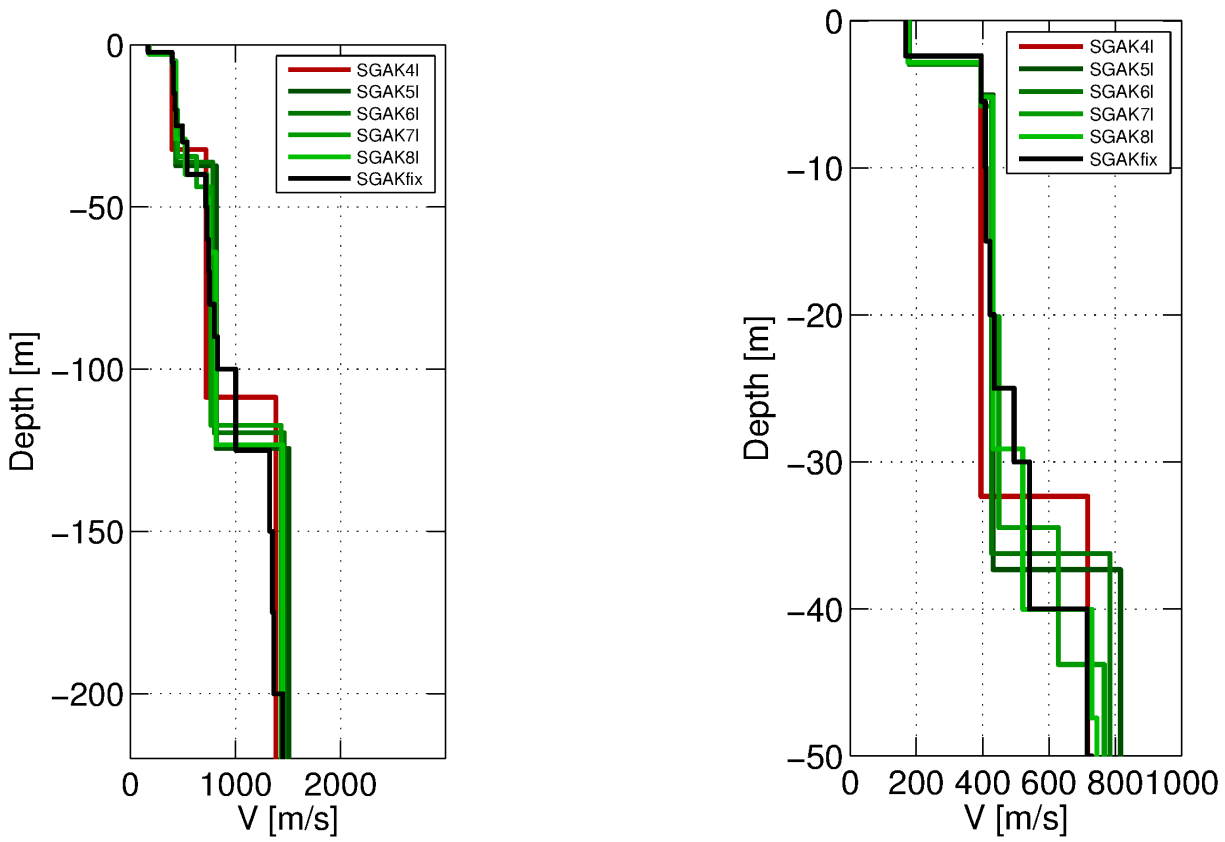

Figure 20: Overview of shear-wave velocity profiles of the best-fitting models of all inversions (left) and a zoom on the shallow part (right).

5.5 SH transfer function

The empirical amplification for station SGAK is already based on 100 events, so the statistical quality of the curve is good. In Fig. 21, the theoretical shear-wave transfer functions for the inversions is compared with the empirical amplification. The empirical amplification shows a double peak at low frequencies, where the theoretical transfer function only shows one broad peak. At the second peak, the frequencies of both curves are in good agreement, but the amplitudes differ. At higher frequencies, the agreement between both curves is striking and the S-wave transfer function fits well with the empirical amplification curve.

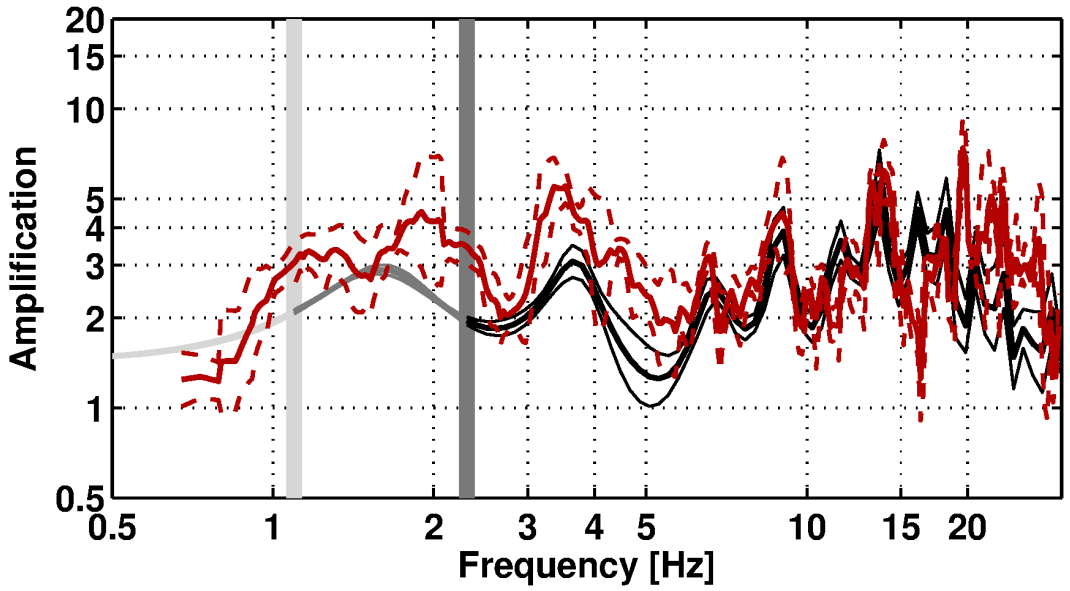

Figure 21: Comparison between the modeled amplification for the best models of the seven different inversions with target 1 (orange, with standard deviation), the inversions with target 2 (blue, with standard deviation) and the empirical amplification measured at station STHK (red, with standard deviation). The vertical light and dark grey bars correspond to the ellipticity peak frequency and the lowest frequency of the dispersion curves, respectively.

5.6 Quarter-wavelength representation

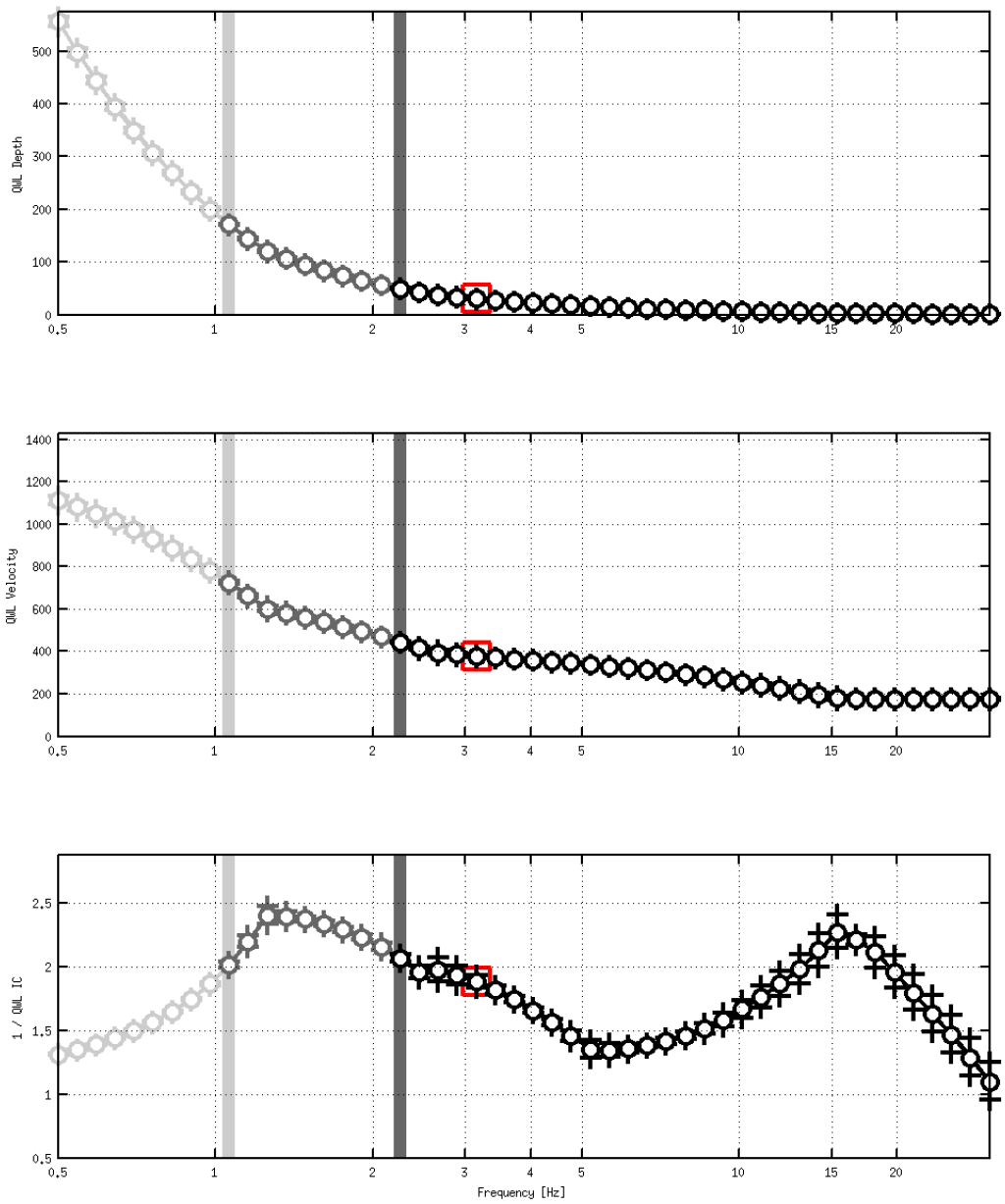

Figure 22: Quarter wavelength representation of the velocity profile for the best models of the inversions (top: depth, center: velocity, bottom: inverse of the impedance contrast). The black curves are constrained by the dispersion curves, the light grey curves are not constrained by the data. The red square corresponds to V_{S30}.

6 Conclusion

We performed a passive array measurement with one array configuration and additional active seismic measurements to characterize the soil underneath station SGAK in Gampel (VS), located on creek deposits at the edge of the Rhône valley.
The dispersion curves for Love and Rayleigh waves could be measured over a wide frequency range, from around 2 to 15 Hz for the Love waves and from about 3 to 20 Hz for the Rayleigh waves using the passive measurements. The active measurements allowed us to measure the Rayleigh wave dispersion curves up to 83 Hz for three different modes. The ellipticity peak frequency was measured at around 2 Hz.
The joint inversion of Love and Rayleigh wave dispersion and ellipticity curves showed that the structure can be explained by models with at least three interfaces. The main features of the structure are a superficial layer of around 3 m thickness with an S-wave velocity of about 175 m/s. The next interface is found at about 37 m depth, where the S-wave velocity increases from about 430 m/s to 785 m/s. The seismic bedrock with a velocity of around 1500 m/s is found at a depth of about 120 m. The V_{S30} of the best models is about 377 m/s, corresponding to soil class B in EC8 and C in SIA261.

Acknowledgements

The authors thank Dario Chieppa for his help during the array measurements.

References

Aki, K. (1957). Space and time spectra of stationary stochastic waves, with special reference to microtremors. *Bull. Earthquake Res. Inst. Tokyo Univ.*, 35:415–456.

Bettig, B., Bard, P.-Y., Scherbaum, F., Riepl, J., Cotton, F., Cornou, C., and Hatzfeld, D. (2001). Analysis of dense array noise measurements using the modified spatial auto-correlation method (SPAC): application to the Grenoble area. *Boll. Geof. Teor. Appl.*, 42:281–304.

Burjánek, J., Gassner-Stamm, G., Poggi, V., Moore, J. R., and Fäh, D. (2010). Ambient vibration analysis of an unstable mountain slope. *Geophys. J. Int.*, 180:820–828.

Burjánek, J., Moore, J. R., Molina, F. X. Y., and Fäh, D. (2012). Instrumental evidence of normal mode rock slope vibration. *Geophys. J. Int.*, 188:559–569.

Fäh, D., Wathelet, M., Kristekova, M., Havenith, H., Endrun, B., Stamm, G., Poggi, V., Burjanek, J., and Cornou, C. (2009). Using ellipticity information for site characterisation. NERIES deliverable JRA4 D4, available at http://www.neries-eu.org.

Hobiger, M., Bard, P.-Y., Cornou, C., and Le Bihan, N. (2009). Single station determination of Rayleigh wave ellipticity by using the random decrement technique (RayDec). *Geophys. Res. Lett.*, 36.

Hobiger, M., Cornou, C., Wathelet, M., Di Giulio, G., Knapmeyer-Endrun, B., Renalier, F., Bard, P.-Y., Savvaidis, A., Hailemikael, S., Le Bihan, N., Ohrnberger, M., and Theodoulidis, N. (2013). Ground structure imaging by inversions of Rayleigh wave ellipticity: Sensitivity analysis and application to European strong motion sites. *Geophys. J. Int.*, 192:201–229.

Maranò, S., Reller, C., Loeliger, H.-A., and Fäh, D. (2012). Seismic waves estimation and wavefield decomposition: Application to ambient vibrations. *Geophys. J. Int.*, 191:175–188.

Park, C. B., Miller, R. D., and Xia, J. (1999). Multichannel analysis of surface waves. *Geophysics*, 64:800–808.

Poggi, V. and Fäh, D. (2010). Estimating Rayleigh wave particle motion from three-component array analysis of ambient vibrations. *Geophys. J. Int.*, 180:251–267.

Redpath, B. B. (1973). Seismic refraction exploration for engineering site investigations. Technical Report E-73-4, National Technical Information Service.

Socco, L. V. and Strobbia, C. (2004). Surface-wave method for near-surface characterization: a tutorial. *Near Surface Geophysics*, 2:165–185.